A Novel Fluorinated Schiff Base: Synthesis, Spectroscopic Characterization, and Quantum Chemical Study

Kamal Raj Sapkota[1*], Vaishali Anand[2], Md. Serajul Haque Faizi[3], Ansu Kumar Roy[4], Rahul Kumar Gupta[5], and Navedul Haque [6]

[1]Department of Chemistry, Tribhuvan University, Prithvi Narayan Campus, Pokhara, Nepal

[2]Department of Chemistry, B.R.M. College, Munger, Bihar, India

[3]Department of Chemistry, Langat Singh College, B.R.A. Bihar University, Muzaffarpur, Bihar

[4]Department of Physics, R.D. & D.J. College, Bihar

[5]Department of Chemistry, Hari Singh College, Haveli Kharagpur, India

[6] Department of Chemistry, B.R.A. Bihar University, India

Submitted: 28 Nov. 2025
Reviewed: 18 Dec. 2025
Accepted : 27 Dec. 2025

DOI: *.10.3126/kdk.v6i1.90110*

Corresponding Author:
Kamal Raj Sapkota
Email: *sapkotakamal69@gmail.com*
Orcid:*https://orcid.org/0009-0006-1274-6880*

कौमोदकी
Kaumodaki
Journal of Multidisciplinary Studies
A Peer-Reviewed, Open Access Journal
ISSN :
2822 - 1567 (Print)
2822 - 1583 (Online)
https://www.nepjol.info/index.php/kdk/about
Published by :
Research Management Cell
Shree Vinduwasini Sanskrit Vidyapeeth (Campus)
Nepal Sanskrit University, Pokhara, Nepal
https://ejournal.vsc.edu.np

Abstract

In this study, we report the design, synthesis, and comprehensive characterization of (E)-N-((1H-pyrrolo[2,3-b]pyridin-4-yl)methylene)-2-fluoro-5-(4H-1,2,4-triazol-4-yl)aniline (PTA), a novel Schiff base integrating three bioactive motifs—pyrrolo[2,3-b]pyridine, 1,2,4-triazole, and fluorinated aniline—linked through a conjugated azomethine group. PTA was synthesized via condensation of 2-fluoro-5-(4H-1,2,4-triazol-4-yl)aniline with 1H-pyrrolo[2,3-b]pyridine-4-carbaldehyde under mild reflux conditions, affording a yellow solid in 81% yield. Its molecular structure was confirmed using Fourier-transform infrared spectroscopy (FT-IR), nuclear magnetic resonance spectroscopy (NMR), ultraviolet–visible spectroscopy (UV–Vis), and mass spectrometry. Density Functional Theory (DFT) analyses, including frontier molecular orbital (FMO) and molecular electrostatic potential (MEP) studies, revealed a HOMO–LUMO gap of 3.562 eV, indicating moderate kinetic stability, and identified regions favorable for electrophilic and nucleophilic interactions. Molecular docking with the sulfonylurea receptor SUR1 (PDB ID: 6PZI) demonstrated stable binding through hydrogen bonding, π–π stacking, and van der Waals interactions, highlighting PTA's potential as an antidiabetic lead. The combined experimental and theoretical findings suggest that PTA's conjugated framework and electronic properties may be exploited in medicinal chemistry and optoelectronic applications.

Keywords: Aniline, azomethine, biological, electronic, nucleophilic

1. Introduction

Heterocyclic compounds having fused N-containing rings have garnered tremendous interest in modern medicinal and material chemistry because of their rich electronic properties, structural variety and a wide range of biological processes (Amin et al., 2022; Nandi et al., 2022; Sahu et al., 2024). Among these, 1H-pyrrolo[2,3-b]pyridine and 1,2,4-triazole motifs stand out as privileged scaffolds in drug design and supramolecular architectures(Amin et al., 2022; Nandi et al., 2022; Sahu et al., 2024; Akter et al., 2024; Mohamed et al., 2014). Pyrrolo[2,3-b]pyridine, a condensed bicyclic heteroaromatic system, displays various pharmacological properties such as kinase inhibition and antiviralactivities(Desai et al., 2023; Dehnavi et al., 2021). Its planar structure and conjugated π-system allow for effective π–π stacking and hydrogen bonding interactions with biological targets, thus enhancing receptor affinity and selectivity(Desai et al., 2023; Dehnavi et al., 2021; Jena et al., 2022; Meyer et al., 2003).

Similarly, the antifungal properties of 1,2,4-triazole derivatives have been thoroughly investigatedantibacterial, anticonvulsant, and antitumor potential(Aggarwal et al., 2012; Kaur et al., 2016; Wang et al., 2022). The electron-deficient nature of the triazole ring and its ability to participate in diverse non-covalent interactions make it an indispensable pharmacophore in modern medicinal chemistry(Zafar et al., 2023; Rusu et al., 2023; Kumar et al., 2024). Introducing fluorine atoms into aromatic frameworks, especially in conjunction with triazoles, significantly alters the physicochemical and pharmacokinetic profiles of organic molecules by increasing lipophilicity, membrane permeability, and metabolic stability(Guan et al., 2024; Kamble et al., 2021; Shabir et al., 2023).

The integration of these heterocycles through a Schiff base linkage (–CH=N–) presents a promising approach for the development of multifunctional compounds with enhanced biological and physicochemical properties(Jadhao et al., 2017; Abdel-Baky et al., 2023; Gong et al., 2016). Schiff bases are known for their facile synthesis, tunable electronic properties, and potential as ligands for coordination chemistry. Moreover, the imine moiety contributes to conjugation and electron delocalization across the molecule, influencing its optical, redox, and electronic behavior(Segura et al., 2016; Kumar et al., 2023; Biswas et al., 2024).

In this work, we provide the creation and synthesis of a novel Schiff base, namely (E)-N-((1H-pyrrolo[2,3-b]pyridin-4-yl)methylene)-2-fluoro-5-(4H-1,2,4-triazol-4-yl)aniline (abbreviated as PTA). The compound features a strategic hybridization of three bioactive moieties: pyrrolo[2,3-b]pyridine, 1,2,4-triazole, and fluorinated aniline, linked through a conjugated azomethine group. The synthetic pathway employed condensation between 2-fluoro-5-(4H-1,2,4-triazol-4-yl)aniline and 1H-pyrrolo[2,3-b]pyridine-4-carbaldehyde under mild conditions.

The structure of the synthesized molecule was clarified and validated using a combination of spectroscopic techniques, including Fourier-transform infrared (FT-IR) spectroscopy, proton and carbon nuclear magnetic resonance (1H and 13C NMR), and ultraviolet-visible (UV-Vis) spectroscopy. Furthermore, using DFT (density functional theory) calculations, frontier molecular orbital (FMO) analysis was performed at the B3LYP/6-311++G(d,p) level to gain understanding of the electronic properties. The HOMO–LUMO energy gap was shown to be a critical component related to the compound's kinetic stability and chemical reactivity.

To further depict the distribution of charges, a molecular electrostatic potential (MEP) map was createdacross the molecule, helping identify electrophilic and nucleophilic regions. These computational studies support the experimental outcomes and furnish a platform for comprehending the electronic structure-activity relationship, which is crucial for future biological and coordination chemistry applications. Additionally, the present work evaluates the antidiabetic potential of the Schiff base ligand (E)-N-((1H-pyrrolo[2,3-b]pyridin-4-yl)methylene)-2-fluoro-5-(4H-1,2,4-triazol-4-yl)aniline (PTA) by exploring its interaction with the sulfonylurea receptor 1 (SUR1). Molecular docking was employed to elucidate the binding behavior and molecular basis of its possible role in modulating insulin secretion.

2. Methods and Materials

2.1. Methods

The functional groups and vibrational features of (E)-N-((1H-pyrrolo[2,3-b]pyridin-4-yl)methylene)-2-fluoro-5-(4H-1,2,4-triazol-4-yl)aniline (PTA) were investigated using Fourier-transform infrared (FT-IR) spectroscopy. A PerkinElmer FT-IR instrument was used to record the spectrum at room temperature (25 °C). For elucidation of the compound's carbon and hydrogen environments, both ^{1}H and ^{13}C nuclear magnetic resonance (NMR) spectra were obtained on a Bruker AVANCE III spectrometer. Additionally, the optical absorption characteristics of PTA were studied through ultraviolet-visible (UV-Vis) spectroscopy, performed on a PerkinElmer Lambda 35 spectrophotometer. Measurements were taken within the 200–600 nm spectral range, using a fixed bandwidth of 1 nm.ESI-MS using a WATERS Q-ToF Premier identified the molecular ion and fragments; elemental composition was verified by CHNS analysis, matching calculated values.

2.2 Materials

Sigma-Aldrich provided all of the reagents used in the synthesis of (E)-N-((1H-pyrrolo[2,3-b]pyridin-4-yl)methylene)-2-fluoro-5-(4H-1,2,4-triazol-4-yl)aniline (PTA), which were used in the reaction exactly as supplied and without further purification.

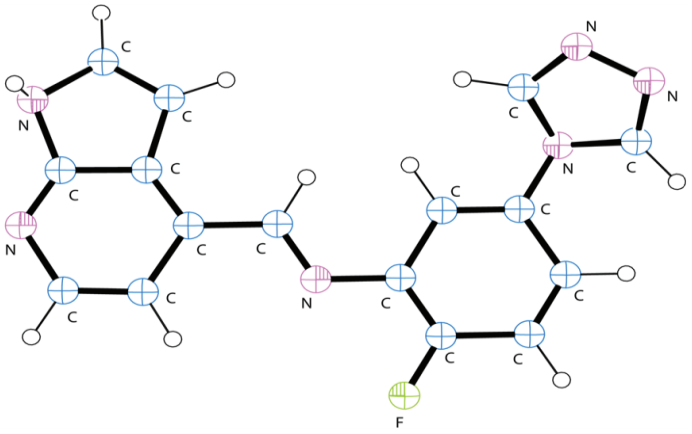

Figure 1 Molecular structure of (E)-N-((1H-pyrrolo[2,3-b]pyridin-4-yl)methylene)-2-fluoro-5-(4H-1,2,4-triazol-4-yl)aniline (PTA)

2.3 **Computational details**

DFT analysis of (E)-N-((1H-pyrrolo[2,3-b]pyridin-4-yl)methylene)-2-fluoro-5-(4H-1,2,4-triazol-4-yl)aniline (PTA) was carried done with Gaussian 09 (Frisch, 2009) with the B3LYP/6-311++G(d,p) theoretical level, following established protocols (Jamal et al., 2024; Murugavel et al., 2019; Hari et al., 2025).). AutoDock Vina and AutoDock Tools (Trott, et al., 2010) were employed to perform the molecular docking study of the target molecule PTA against SUR1.

3. Results and conversation

3.1 Synthesis of (E)-N-((1H-pyrrolo[2,3-b]pyridin-4-yl)methylene)-2-fluoro-5-(4H-1,2,4-triazol-4-yl)aniline (PTA).

PTA was synthesized by reacting 2-fluoro-5-(4H-1,2,4-triazol-4-yl)aniline (1) with 1H-pyrrolo[2,3-b]pyridine-4-carbaldehyde (2), as shown in Scheme 1. 20 mL of methanol was used to dissolve 0.60 g (3.36 mmol) of 2-fluoro-5-(4H-1,2,4-triazol-4-yl)aniline, and 0.50 g (3.42 mmol) of 1H-pyrrolo[2,3-b]pyridine-4-carbaldehyde was then added to the process. After eight hours of refluxing the combination, the solvent volume dropped to 10 mL, forming a pale yellow precipitate. The solid was then isolated by filtration, purified by washing with cold methanol (5 mL) and hexane (10 mL), and recrystallized from methanol. The product was dried under a vacuum to give a yellow solid.Finally, the PTA was obtained as a yellow solid with a yield of 0.90 g, corresponding to 81%. The structure of PTA is shown in Figure 1.

The elemental composition of (E)-N-((1H-pyrrolo[2,3-b]pyridin-4-yl)methylene)-2-fluoro-5-(4H-1,2,4-triazol-4-yl)aniline (PTA) was confirmed through elemental analysis. The experimentally determined percentages were found to be: carbon (C), 62.74%;

hydrogen (H), 3.62%; fluorine (F), 6.20%; and nitrogen (N), 27.44%. These values are in good agreement with the theoretically calculated values, which were: C, 62.54%; H, 3.51%; F, 6.15%; and N, 27.38%, indicating the high purity of the synthesized compound. The close match between the observed and calculated values supports the proposed molecular formula ($C_{16}H_{11}FN_6$) and confirms the successful synthesis of PTA.

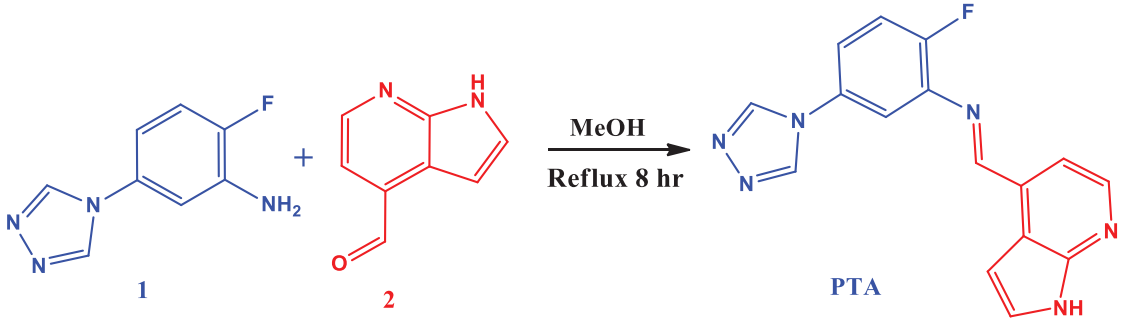

Scheme 1

3.2 NMR study

3.2.1 ^{1}H NMR

^{1}H NMR (400 MHz, DMSO-d$_6$, δ in ppm): The ^{1}H NMR (nuclear magnetic resonance) spectrum (Figure 2) displays two characteristic downfield singlets in the region δ 9.85–9.10 ppm, which may attributed to the imine proton (–CH=N–) and the NH proton of the triazole or pyrrole ring(Pavia et al., 2015; Pretsch et al., 2013). A broad singlet is observed between δ 8.80–8.40 ppm, corresponding to the proton on the triazole ring. A sharp singlet around δ 8.10 ppm is likely due to an aromatic proton positioned adjacent to the fluorine-substituted aniline ring(Pavia et al., 2015; Pretsch et al., 2013; Sharma, 2007). In the region of δ 7.90–7.10 ppm, multiple signals are seen: a small singlet and a weakly resolved triplet, which are assigned to the aromatic protons of the pyrrolo[2,3-b]pyridine and aniline moieties, showing the expected splitting patterns due to neighboring protons(Pavia et al., 2015; Pretsch et al., 2013; Sharma, 2007; Field et al., 2013). A prominent peak at δ 3.50 ppm corresponds to the residual DMSO-d$_6$ solvent. The overall splitting and chemical shifts are consistent with the structure of PTA, confirming the presence of conjugated heteroaromatic systems and the imine linkage.

3.2.2 ^{13}C NMR

^{13}C NMR (100 MHz, DMSO-d$_6$, δ in ppm):The ^{13}C NMR spectrum (Figure 2) of PTA exhibits a total of 14 distinct carbon resonances, consistent with the proposed structure. Two prominent signals are observed in the downfield region between δ 160–170 ppm, which are attributed to the imine carbon (–CH=N–) and the fluorinated aromatic carbon, both typically deshielded due to the presence of electronegative atoms(Pretsch et al., 2013; Sharma, 2007). Four additional peaks appear in the δ 160–140 ppm range, corresponding to heteroaromatic carbons in the triazole and pyrrolo[2,3-b]pyridine

rings(Pavia et al., 2015; Field et al., 2013). Five peaks between δ 140–120 ppm are assigned to protonated aromatic carbons within the aniline and fused heterocyclic systems. Three more signals are located in the δ 120–100 ppm region, consistent with the remaining aromatic carbon atoms(Murugavel et al., 2019; Pavia et al., 2015; Sharma, 2007; Field et al., 2013). A singlet near δ 39.5 ppm is observed due to the residual DMSO-d_6 solvent. The overall pattern supports the presence of conjugated aromatic and heteroaromatic frameworks, along with the imine functionality, and aligns well with the expected chemical environment of the PTA molecule.

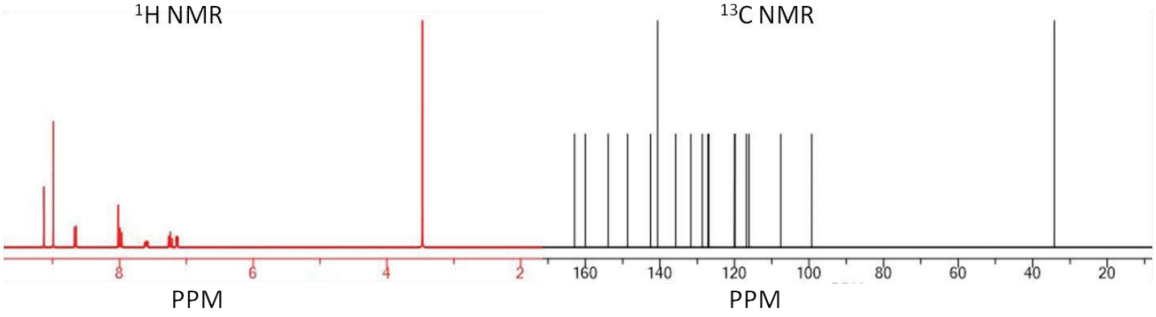

Figure 2. NMR spectrum of PTA showing the –CH=N– signal and aromatic/heterocyclic protons, confirming its structure.

3.3 FT-IR Study

The FT-IR (Fourier-transform infrared) spectrum (Figure 3) of (E)-N-((1H-pyrrolo[2,3-b]pyridin-4-yl)methylene)-2-fluoro-5-(4H-1,2,4-triazol-4-yl)aniline (PTA) exhibits several characteristic absorption bands that confirm the presence of key functional groups in the molecule (Figure 3). A weak and broad band around 3500 cm^{-1} corresponds to the N–H stretching vibration, likely from the triazole or pyrrole NH group(Pavia et al., 2015; Socrates, 2004). Peaks at 3136 and 3052 cm^{-1} are attributed to aromatic C–H stretching vibrations, while bands observed at 2982, 2911, and 2848 cm^{-1} are caused by C-H stretching in aliphatic and aromatic compounds, indicating the presence of multiple aromatic and heteroaromatic rings(Sharma, 2007; Socrates, 2004). A sharp and intense peak at 1678 cm^{-1} confirms the C=N's existence stretching vibration of the imine (Schiff base) linkage(Pavia et al., 2015; Socrates, 2004). The peaks at 1617, 1588, 1527, 1491, and 1445 cm^{-1} are associated with aromatic C=C stretching and skeletal vibrations of the fused heterocyclic system. Peaks in the region of 1395 and 1369 cm^{-1} may correspond to C–N stretching and in-plane bending of the aromatic system. Strong absorptions between 1254–1174 cm^{-1} (specifically at 1254, 1248, 1227, 1210, and 1174 cm^{-1}) are characteristic of C–F stretching and C–N vibrations, while bands at 1099, 1073, and 1009 cm^{-1} may be due to ring breathing modes or C–H in-plane bending(Jamal et al., 2024; Murugavel et al., 2019; Pavia et al., 2015; Socrates, 2004). Additional peaks at 954, 914, 761, 693, and 668 cm^{-1} can be assigned to the aromatic rings' out-of-plane C–H bending vibrations. The lower frequency peaks at 557 and 454 cm^{-1} are attributed to skeletal

bending and ring deformation modes (Socrates, 2004; Pavia et al., 2015; Sapkota et al., 2025). These vibrational features collectively confirm the presence of imine, triazole, pyridine, fluorinated aniline, and pyrrole functionalities in PTA, supporting its proposed structure.

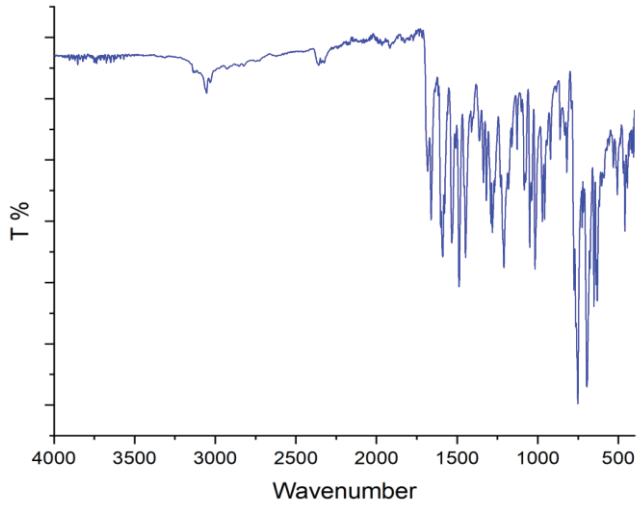

Figure 3. FT-IR spectrum of PTA displaying key functional groups, including the –C=N– stretching and aromatic/heterocyclic vibrations, supporting the proposed structure.

3.4 UV–Vis study

The absorption spectra of UV-Vis (ultraviolet-visible) of (E)-N-((1H-pyrrolo[2,3-b]pyridin-4-yl)methylene) (PTA) were recorded in methanol to investigate its electronic transitions and assess the extent of π-conjugation within the molecular framework (Figure 4). The spectrum revealed a strong and well-defined absorption maximum (λmax) at 353 nm, which is characteristic of a π→π* transition (Pavia et al., 2015; Sharma, 2007; Qian et al., 2015). This band is primarily attributed to the extended delocalization of π-electrons across the conjugated system involving the imine linkage (–CH=N–), the electron-rich pyrrolo[2,3-b]pyridine unit, the triazole moiety, and the fluorinated aniline ring. The absorption at 353 nm occurs in the near-ultraviolet (near-UV) region, which refers to light with wavelengths just below the visible spectrum, typically between 300–400 nm. In simpler terms, this means the molecule absorbs light that is slightly higher in energy than visible light, which can be detected using standard UV–Vis spectroscopy. The presence of this absorption band supports the formation of a highly conjugated and planar system within the molecule, enhancing its ability to absorb light in the lower-energy region of the UV spectrum (Pavia et al., 2015; Sharma, 2007). The slight bathochromic (red) shift observed, compared to simple aromatic or non-conjugated systems, indicates increased conjugation and electron delocalization introduced by the imine functionality and heteroaromatic rings (Pavia et al., 2015; Pretsch et al., 2013;

Sharma, 2007). The fluorine substitution on the aniline ring and the nitrogen-rich triazole group may also contribute to stabilization of the excited state, further influencing the electronic transition energy (Pavia et al., 2015; Sharma, 2007). Overall, the UV–Vis spectral data support the structural features proposed for PTA and provide evidence of its conjugated π-electron system. The absorption at 353 nm suggests potential utility in optoelectronic or biological applications where extended conjugation and light absorption are relevant.

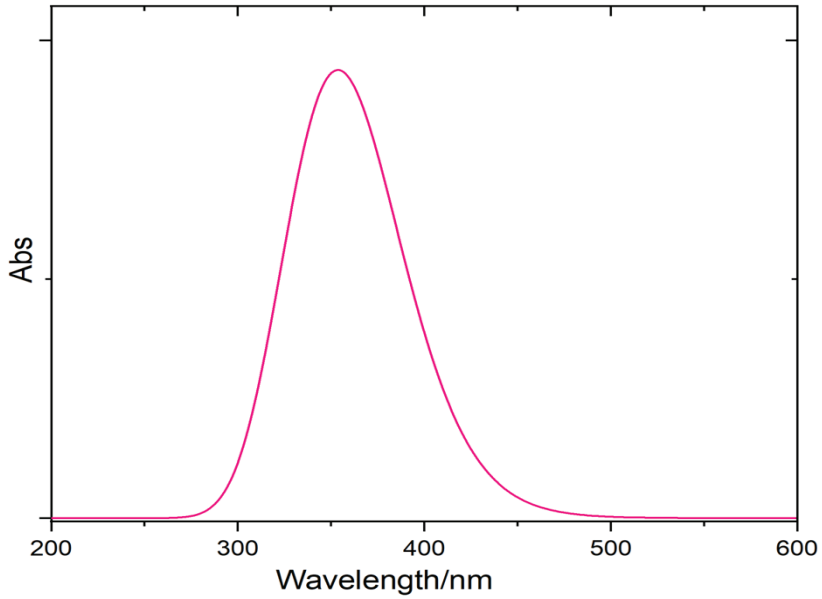

Figure 4. UV-Vis spectrum of PTA showing a π→π* absorption at 353 nm, confirming extended π-conjugation.

3.5 Analysis of Frontier Molecular Orbitals (FMO)

Analysis of the Frontier Molecular Orbital (FMO) is a crucial theoretical technique for comprehending molecules' electronic properties and reactivity profile, particularly in the context of electron transfer, excitation phenomena, and interaction with biological targets(Jamal et al., 2024; Murugavel et al., 2019; Sengupta et al., 2022; Jamal et al., 2024). In the present study, the FMO analysis of (E)-N-((1H-pyrrolo[2,3-b]pyridin-4-yl)methylene)-2-fluoro-5-(4H-1,2,4-triazol-4-yl)aniline (PTA) was carried out to evaluate its chemical reactivity and kinetic stability. As shown in the HOMO–LUMO diagram (Figure 5**)**, the energies of the HOMO and LUMO were found to be −5.513 eV and −1.951 eV, respectively, with an energy gap of 3.562 eV. The resulting HOMO–LUMO gap in energy (ΔE) was discovered to be 3.562 eV, indicating a moderate kinetic stability and relatively low chemical reactivity of the molecule. Because a smaller gap denotes greater reactivity and lesser stability and a larger gap denotes the opposite, this energy gap is an important characteristic. (Jamal et al., 2024; 2024). Again, the experimental

absorption maximum (λ_{max}) for PTA was recorded at 353 nm, corresponding to an electronic excitation energy of approximately 3.51 eV. As shown in the HOMO–LUMO energy diagram (Figure 5), this value is in close agreement with the calculated energy gap, thereby supporting the reliability of the FMO analysis. This excellent correlation between the calculated energy gap and the experimental λ_{max} substantiates the reliability of the computational method employed and suggests that the dominant transition contributing to the absorption is the HOMO → LUMO transition. The HOMO is predominantly localized over the electron-donating moieties such as the aniline and pyrrolopyridine rings, whereas the LUMO is mainly delocalized over the electron-deficient triazole ring and adjacent π-system. This spatial separation implies an intramolecular charge transfer (ICT) upon excitation, which may enhance the molecule's interaction with biological targets and its optoelectronic behavior(Jamal et al., 2024; Murugavel et al., 2019; Jamal et al., 2024; Samanta et al., 2023). The FMO study emphasizes PTA as a molecule with favorable electronic characteristics for potential medicinal chemistry and molecular electronics applications.

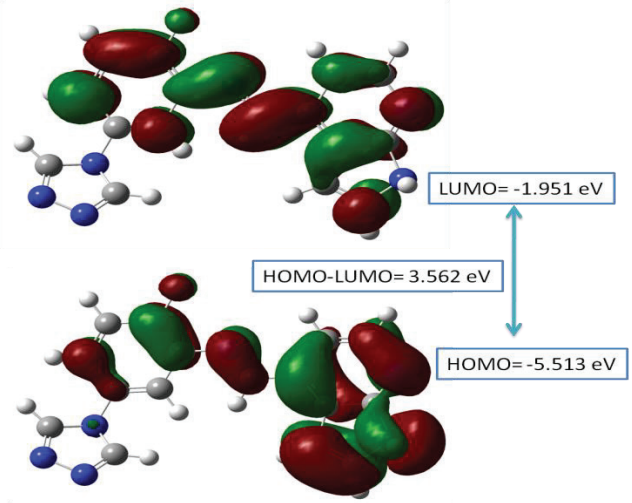

Figure 5. Frontier molecular orbitals (HOMO and LUMO) of PTA, showing the HOMO localized on electron-donating pyrrolopyridine and aniline units and the LUMO delocalized over the triazole ring, indicating intramolecular charge transfer and a HOMO–LUMO gap of 3.562 eV.

3.6 Analysis of Molecular Electrostatic Potential (MEP)

The map of the molecular electrostatic potential (MEP) of (E)-N-((1H-pyrrolo[2,3-b]pyridin-4-yl)methylene)-2-fluoro-5-(4H-1,2,4-triazol-4-yl)aniline (PTA) provides a valuable visualization of the charge distribution across the molecular surface, aiding in the prediction of reactive sites and molecular interactions. The MEP surface was computed and color-coded over an electrostatic potential range of -6.699×10^{-2} to $+6.699 \times 10^{-2}$ a.u., with red representing regions of maximum negative potential and blue

(or white, in this case) indicating areas of maximum positive potential. In the MEP map of PTA, red and yellow regions are prominently observed on electronegative atoms—specifically, the nitrogen atoms of the triazole and pyrrolopyridine rings, as well as the fluorine atom on the aromatic ring. These areas represent zones of high electron density and negative electrostatic potential, making them favorable sites for electrophilic interactions. The intense red over the nitrogen atoms suggests a strong nucleophilic character, contributing to hydrogen bonding potential and possible interactions with electrophilic sites in biological targets. Green regions, which indicate regions of nearly zero electrostatic potential, are primarily localized on the hydrogen atoms. This neutrality suggests a balanced electron distribution in these regions and points to low chemical reactivity. These hydrogen atoms could participate in weak van der Waals or hydrogen bonding interactions depending on the molecular environment. The white regions correspond to carbon atoms, mainly in the aromatic and heteroaromatic rings, reflecting areas of low electron density and slight positive electrostatic potential(Jamal et al., 2024; Murugavel et al., 2019; Remya et al., 2016). These carbon atoms are typically chemically stable and not reactive toward electrophiles or nucleophiles under standard conditions. The electrostatic surface demonstrates an effective charge separation, emphasizing the molecule's dipolar character. This polarity, conjoined with the existence of both electron-rich and neutral areas, enhances the potential of PTA to participate in various non-covalent interactions, which is important in molecular recognition and biological activity.

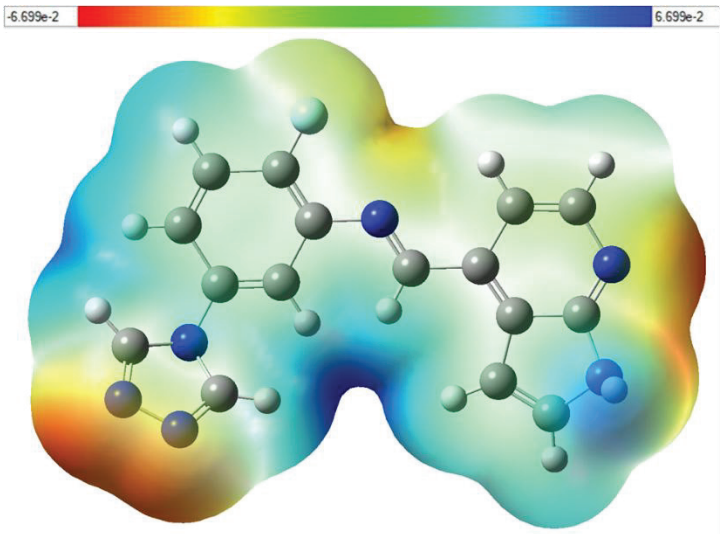

Figure 6. MEP map of PTA showing electron-rich regions (red) over N and F atoms and electron-deficient/neutral regions (green/white) on H and C atoms, indicating charge distribution and reactive sites.

3.7 Docking

The molecular docking simulation of (E)-N-((1H-pyrrolo[2,3-b]pyridin-4-yl)methylene)-2-fluoro-5-(4H-1,2,4-triazol-4-yl)aniline (PTA) with the sulfonylurea receptor SUR1 (PDB ID: 6PZI**)** (Martin et al., 2019) generated nine plausible binding conformations with predicted binding energies ranging from −6.7 to −5.9 kcal/mol, indicating a favorable and consistent interaction profile (Table 1). Among these, Mode 1 exhibited the lowest binding energy **(**−6.7 kcal/mol) and was therefore selected as the most stable and energetically preferred conformation, showing **zero RMSD** relative to itself. The remaining docking poses displayed only marginally higher binding affinities (−6.6 to −6.2 kcal/mol), with RMSD values ranging from 2.665 to 10.116 **Å**, reflecting reasonable conformational diversity while maintaining comparable energetic feasibility. The narrow distribution of binding energies ($\Delta G \leq 0.8$ kcal/mol) suggests that PTA is capable of adopting multiple stable orientations within the SUR1 binding pocket, a feature commonly associated with ligands stabilized through a combination of hydrogen bonding and hydrophobic interactions (Bukhari et al., 2026; Murugavel et al., 2019; Jamal et al., 2025). The best-ranked docking pose demonstrated excellent geometric complementarity with the active-site residues of SUR1 and was stabilized by a network of non-covalent interactions, including conventional hydrogen bonds, π–π stacking, and van der Waals forces, which collectively enhance the stability of the ligand–receptor complex (Figure 7). Such interactions are consistent with those observed for known sulfonylurea drugs that exert their antidiabetic effects by modulating the activity of ATP-sensitive potassium channels. Overall, the docking energy distribution, RMSD analysis, and interaction pattern confirm that PTA forms a stable and energetically favorable complex with SUR1, supporting its potential as a promising antidiabetic lead compound and providing a strong molecular basis for further experimental and pharmacological validation.

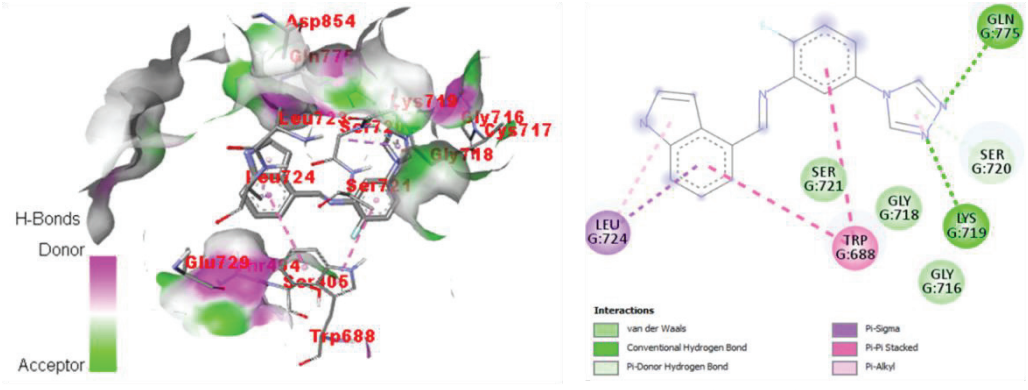

Figure 7. Docked pose of PTA in the binding site of SUR1 (PDB ID: 6PZI).

Table 1. Docking scores and RMSD values of PTA with SUR1 (PDB ID: 6PZI).

mode	Affinity (kcal/mol)	rmsd l.b.	rmsd u.b.
1	-6.7	0.000	0.000
2	-6.6	4.914	9.031
3	-6.5	5.929	10.116
4	-6.4	4.072	8.165
5	-6.3	5.654	9.827
6	-6.2	5.950	8.749
7	-6.2	3.349	4.361
8	-6.0	3.295	7.423
9	-5.9	2.665	3.886

4. Conclusion

With an 81% yield, or 0.90 g of the yellow solid, (E)-N-((1H-pyrrolo[2,3-b] pyridin-4-yl) methylene)-2-fluoro-5-(4H-1,2,4-triazol-4-yl) aniline (PTA) was synthesized. The elemental analysis confirmed the molecular formula C16H11FN6, with the observed elemental composition being: C, 62.74%; H, 3.62%; F, 6.20%; and N, 27.44%, closely matching the calculated values of C, 62.54%; H, 3.51%; F, 6.15%; and N, 27.38%. NMR spectra, including ^{1}H NMR and ^{13}C NMR, supported the presence of key functional groups and confirmed the expected molecular structure. The FT-IR spectrum showed characteristic bands corresponding to N–H stretching, C=N stretching, and C–F vibrations. The UV–Vis spectrum displayed a strong absorption at 353 nm, attributed to the $\pi \rightarrow \pi^*$ transition. The molecular ion peak in the mass spectrum at m/z 306.10 confirmed the molecular weight. FMO analysis indicated a HOMO–LUMO gap of 3.562 eV, aligning with the experimental λmax of 353 nm, suggesting electronic stability and potential for interaction with biological targets. The MEP map indicated that the negative electrostatic potential is primarily localized on PTA's nitrogen and fluorine atoms, suggesting sites for electrophilic interactions, while docking studies showed favorable binding to the SUR1 receptor (−6.7 kcal/mol) through stable interactions with key active-site residues, supporting its potential as an antidiabetic lead.

References

Abdel-Baky, Y. M., Omer, A. M., El-Fakharany, E. M., Ammar, Y. A., Abusaif, M. S., & Ragab, A. (2023). Developing a new multi-featured chitosan-quinoline Schiff base with potent antibacterial, antioxidant, and antidiabetic activities: Design and molecular modeling simulation. *Scientific Reports*, 13(1), 22792.

Aggarwal, R., &Sumran, G. (2020). An insight on medicinal attributes of 1, 2, 4-triazoles. *European Journal of Medicinal Chemistry*, 205, 112652.

Akter, M., Rupa, K., &Anbarasan, P. (2022). 1,2,3-Triazole and its analogues: new surrogates for diazo compounds. *Chemical Reviews*, 122(15), 13108-13205.

Amin, A., Qadir, T., Sharma, P. K., Jeelani, I., & Abe, H. (2022). A review on the medicinal and industrial applications of N-containing heterocycles. *The Open Medicinal Chemistry Journal*, 16(1).

Biswas, T., Mittal, R. K., Sharma, V., Kanupriya, & Mishra, I. (2024). Schiff bases: versatile mediators of medicinal and multifunctional advancements. *Letters in Organic Chemistry*, 21(6), 505-519.

Bukhari, K., Alharbi, R. S., Alharbi, B. F., Alwanian, W. M., Alharbi, H. O., Mackawy, A. M., ... & Allemailem, K. S. (2026). Targeting the 2'-O-Methyltransferase Activity of SARS-CoV-2 nsp16 Through Discovery of Small Molecule Inhibitors Via an Integrated Computational Approach. *Journal of Pharmaceutical Innovation*, 21(1), 31.

Dehnavi, F., Alizadeh, S. R., &Ebrahimzadeh, M. A. (2021). Pyrrolopyrazine derivatives: Synthetic approaches and biological activities. *Medicinal Chemistry Research*, 1–26.

Desai, N. C., Monapara, J. D., Jethawa, A. M., & Pandit, U. (2023). Contemporary development in the synthesis and biological applications of pyridine-based heterocyclic motifs. *In Recent Developments in the Synthesis and Applications of Pyridines* (pp. 253–298). Elsevier.

Field, L. D., Sternhell, S., & Kalman, J. R. (2013). *Organic structures from spectra*. John Wiley & Sons.

Frisch, M. J. E. A. (2009). *Gaussian 09, Revision D.01, Gaussian Inc*., Wallingford, CT.

Gong, H. H., Addla, D., Lv, J. S., & Zhou, C. H. (2016). Heterocyclic naphthalimides as new skeleton structure of compounds with increasingly expanding relational medicinal applications. *Current Topics in Medicinal Chemistry*, 16(28), 3303–3364.

Guan, Q., Xing, S., Wang, L., Zhu, J., Guo, C., Xu, C., ... & Sun, H. (2024). Triazoles in medicinal chemistry: physicochemical properties, bioisosterism, and application. *Journal of Medicinal Chemistry*, 67(10), 7788–7824.

Hari, K. C., Neupane, K., Chhetri, K. B., Ojha, R., & Acharya, R. K. (2025). Molecular docking and density functional theory studies of flavonoids of Holy basil plant against COX-2 enzyme. *Biophysical chemistry*, 107533.

Jamal, A., Faizi, M. S. H., &Necmi, D. E. G. E. (2024). Synthesis, structural characterization, DFT calculations, and molecular docking of a novel quinoline derivative. *Journal of Molecular Structure*, 1300, 137251.

Jamal, A., Ferjani, H., Faizi, M. S. H., &Alzahrani, A. Y. A. (2024). DFT calculation and molecular docking studies of designing quinoline-derived anti-Alzheimer agents with NLO response. *Journal of the Indian Chemical Society*, 101(8), 101181.

Jamal, A., Faizi, M. S. H., & Roy, A. K. (2025). Synthesis, Crystal Structure, and Spectroscopic Study of a Novel Quinoline Derivative with Nonlinear Optical Activity and Esterase Inhibition Potential. *Journal of Molecular Structure*, 144407.

Jadhao, M., Das, C., Rawat, A., Kumar, H., Joshi, R., Maiti, S., & Ghosh, S. K. (2017). Development of multifunctional heterocyclic Schiff base as a potential metal

chelator: a comprehensive spectroscopic approach towards drug discovery. JBIC *Journal of Biological Inorganic Chemistry*, 22, 47–59.

Jena, S., Dutta, J., Tulsiyan, K. D., Sahu, A. K., Choudhury, S. S., & Biswal, H. S. (2022). Noncovalent interactions in proteins and nucleic acids: Beyond hydrogen bonding and π-stacking. *Chemical Society Reviews*, 51(11), 4261–4286.

Kamble, O., Dandela, R., & Shinde, S. (2021). Recent Innovations of Organo-fluorine Synthesis and Pharmacokinetics. *Current Organic Chemistry*, 25(21), 2650–2665.

Kaur, R., Ranjan Dwivedi, A., Kumar, B., & Kumar, V. (2016). *Recent developments on 1,2,4-triazole nucleus in anticancer compounds: a review*. Anti-Cancer Agents in Medicinal Chemistry, 16(4), 465–489.

Kumar Harish, K., Kamat, V., Nagaraja, O., NelligereRevanna, B., Rajeena, C. A., &Madegowda, M. (2024). Probing the hybridized triazole-chalcones: an in-depth investigations of molecular structure journey towards antibacterial potential against DNA gyrase. *Journal of Biomolecular Structure and Dynamics*, 1–30.

Kumar, M., Singh, A. K., Singh, A. K., Yadav, R. K., Singh, S., Singh, A. P., & Chauhan, A. (2023). Recent advances in 3d-block metal complexes with bi, tri, and tetradentate Schiff base ligands derived from salicylaldehyde and its derivatives: Synthesis, characterization and applications. *Coordination Chemistry Reviews*, 488, 215176.

Martin, G. M., Sung, M. W., Yang, Z., Innes, L. M., Kandasamy, B., David, L. L., et al. (2019). Mechanism of pharmacochaperoning in a mammalian KATP channel revealed by Cryo-EM. *eLife*, 8, e46417.

Meyer, E. A., Castellano, R. K., &Diederich, F. (2003). Interactions with aromatic rings in chemical and biological recognition. *AngewandteChemie International Edition*, 42(11), 1210–1250.

Murugavel, S., Ravikumar, C., Jaabil, G., &Alagusundaram, P. (2019). Synthesis, crystal structure analysis, spectral investigations (NMR, FT-IR, UV), DFT calculations, ADMET studies, molecular docking and anticancer activity of 2-(1-benzyl-5-methyl-1H-1,2,3-triazol-4-yl)-4-(2-chlorophenyl)-6-methoxypyridine–a novel potent human topoisomerase IIα inhibitor. *Journal of Molecular Structure*, 1176, 729–742.

Nandi, S., Jamatia, R., Sarkar, R., Sarkar, F. K., Alam, S., & Pal, A. K. (2022). One-Pot Multicomponent Reaction: A Highly Versatile Strategy for the Construction of Valuable Nitrogen-Containing Heterocycles. *ChemistrySelect*, 7(33), e202201901.

Pavia, D. L., Lampman, G. M., Kriz, G. S., & Vyvyan, J. R. (2015). *Introduction to Spectroscopy.*

Qian, X., Zhu, Y. Z., Chang, W. Y., Song, J., Pan, B., Lu, L., ... & Zheng, J. Y. (2015). Benzo[a]carbazole-based donor−π–acceptor type organic dyes for highly efficient dye-sensitized solar cells. *ACS Applied Materials & Interfaces*, 7(17), 9015–9022.

Pretsch, E., Clerc, T., Seibl, J., & Simon, W. (2013). *Tables of Spectral Data for Structure Determination of Organic Compounds*. Springer Science & Business Media.

Remya, G. S., & Suresh, C. H. (2016). Quantification and classification of substituent effects in organic chemistry: A theoretical molecular electrostatic potential study. *Physical Chemistry Chemical Physics*, 18(30), 20615–20627.

Rusu, A., Moga, I. M., Uncu, L., &Hancu, G. (2023). The role of five-membered heterocycles in the molecular structure of antibacterial drugs used in therapy. *Pharmaceutics*, 15(11), 2554.

S Mohamed, M., & S Fathallah, S. (2014). Pyrroles and fused pyrroles: synthesis and therapeutic activities. *Mini-Reviews in Organic Chemistry*, 11(4), 477–507.

Sahu, B., Verma, M., Thakur, A., Bharti, R., & Sharma, R. (2024). TBAB in One-pot Green Approach for the Synthesis of N-Heterocyclic Compounds: A Comprehensive Review. *Current Chinese Science*, 4(1), 2–24.

Samanta, P. K., & Misra, R. (2023). Intramolecular charge transfer for optical applications. *Journal of Applied Physics*, 133(2).

Sapkota, K. R., Begam, J., & Kumari, S. (2025). A Novel Imidazole Derivative: Synthesis, Spectral Characterization, and DFT Study. *AMC Multidisciplinary Research Journal*, 4(1), 79-88.

Segura, J. L., Mancheño, M. J., & Zamora, F. (2016). Covalent organic frameworks based on Schiff-base chemistry: synthesis, properties and potential applications. *Chemical Society Reviews*, 45(20), 5635–5671.

Sengupta, A., Li, B., Svatunek, D., Liu, F., &Houk, K. N. (2022). Cycloaddition reactivities analyzed by energy decomposition analyses and the frontier molecular orbital model. *Accounts of Chemical Research*, 55(17), 2467–2474.

Sharma, Y. R. (2007). *Elementary Organic Spectroscopy*. S. Chand Publishing.

Shabir, G., Saeed, A., Zahid, W., Naseer, F., Riaz, Z., Khalil, N., ... &Albericio, F. (2023). Chemistry and pharmacology of fluorinated drugs approved by the FDA (2016–2022). *Pharmaceuticals*, 16(8), 1162.

Socrates, G. (2004). *Infrared and Raman Characteristic Group Frequencies*: Tables and Charts. John Wiley & Sons.

Trott, O., & Olson, A. J. (2010). AutoDock Vina: Improving the speed and accuracy of docking with a new scoring function, efficient optimization, and multithreading. *Journal of Computational Chemistry*, 31(2), 455–461

Wang, Y., & Liu, D. (2022). An important potential anti-epileptic/anticonvulsant active group: a review of 1,2,4-triazole groups and their action. *Drug Research*, 72(03), 131–138.

Zafar, W., Ashfaq, M., &Sumrra, S. H. (2023). A review on the antimicrobial assessment of triazole-azomethine functionalized frameworks incorporating transition metals. *Journal of Molecular Structure*, 1288, 135744.